Ions in the Thermosphere of Exoplanets: Observable Constraints Revealed by Innovative Laboratory Experiments

Jérémy Bourgalais, Nathalie Carrasco, Quentin Changeat, Olivia Venot, Lora Jovanovic, Pascal Pernot, Jonathan Tennyson, Katy Chubb, Sergey Yurchenko, Giovanna Tinetti

Draft version April 28, 2020
Typeset using LaTeX **manuscript** style in AASTeX63

Ions in the Thermosphere of Exoplanets: Observable Constraints Revealed by Innovative Laboratory Experiments

Jérémy Bourgalais,[1] Nathalie Carrasco,[1] Quentin Changeat,[2] Olivia Venot,[3] Lora Jovanović,[1] Pascal Pernot,[4] Jonathan Tennyson,[2] Katy L. Chubb,[2,5] Sergey N. Yurchenko,[2] and Giovanna Tinetti[2]

[1]*LATMOS/IPSL, UVSQ, Université Paris-Saclay, UPMC Univ. Paris 06, CNRS, Guyancourt, France.*

[2]*Department of Physics & Astronomy, University College London, Gower Street, WC1E 6BT London, United Kingdom.*

[3]*Laboratoire Interuniversitaire des Systèmes Atmosphériques (LISA), UMR CNRS 7583, Université Paris-Est-Créteil, Université de Paris, Institut Pierre Simon Laplace, Créteil, France.*

[4]*Laboratoire de Chimie Physique, CNRS, Univ. Paris-Sud, Université Paris-Saclay, 91405, Orsay, France.*

[5]*SRON Netherlands Institute for Space Research, Sorbonnelaan 2, 3584 CA, Utrecht, Netherlands.*

(Received XXX X, 20XX; Revised XXX X, 20XX; Accepted April 17th, 2020)

Submitted to The Astrophysical Journal

ABSTRACT

With the upcoming launch of space telescopes dedicated to the study of exoplanets, the *Atmospheric Remote-Sensing Infrared Exoplanet Large-survey* (ARIEL) and the *James Webb Space Telescope* (JWST), a new era is opening in the exoplanetary atmospheric explorations. However, especially in relatively cold planets around later-type stars, photochemical hazes and clouds may mask the composition of the lower part of the atmosphere, making it difficult to detect any chemical species in the troposphere or to

Corresponding author: Jérémy Bourgalais
jeremy.bourgalais@latmos.ipsl.fr

understand whether there is a surface or not. This issue is particularly exacerbated if the goal is to study the habitability of said exoplanets and to search for biosignatures.

This work combines innovative laboratory experiments, chemical modeling and simulated observations at ARIEL and JWST resolutions. We focus on the signatures of molecular ions that can be found in upper atmospheres above cloud decks. Our results suggest that H_3^+ along with H_3O^+ could be detected in the observational spectra of sub-Neptunes based on realistic mixing ratio assumption. This new parametric set may help to distinguish super-Earths with a thin atmosphere from H_2-dominated sub-Neptunes, to address the critical question whether a low-gravity planet around a low-mass active star is able to retain its volatile components. These ions may also constitute potential tracers to certain molecules of interest such as H_2O or O_2 to probe the habitability of exoplanets. Their detection will be an enthralling challenge for the future JWST and ARIEL telescopes.

Keywords: planets and satellites: atmospheres — methods: laboratory — ultraviolet: planetary systems — molecular processes

1. INTRODUCTION

Thanks to the Kepler mission (Borucki 2016), many exoplanets of a new kind, bigger than the Earth but smaller than Neptune ($1R_\oplus < R_p < 4R_\oplus$) have been observed and constitute the majority of the worlds detected outside the solar system (Coughlin et al. 2016). Based on observations and theoretical considerations, many of these low-gravity planets seem to have thick atmospheres which retain light species (H_2, He) (Jontof-Hutter 2019). However, these small planets show a great diversity of densities, suggesting a diverse range of bulk and atmospheric compositions including rocky planets with thin atmospheres mainly made of heavy molecules such as N_2, CO, or H_2O (Rimmer & Rugheimer 2019; Hu & Seager 2014; Moses et al. 2013; Elkins-Tanton & Seager 2008; Schaefer et al. 2012).

These atmospheric constituents have a significant impact on the evolution of the planet, including its potential habitability. Many low-gravity planets are detected mainly in orbit around low-mass M-type stars which are the most abundant stars in our galaxy (Laughlin et al. 2004; Chabrier 2003). These stars emit strongly in the UltraViolet (UV) and the atmospheric properties as well as the dynamics and fate of their associated exoplanets are thus strongly impacted by stellar radiation (Shkolnik & Barman 2014). Based on our current knowledge of the solar system's bodies, such as Titan (Hörst 2017), high-energy radiation, in particular in the Extreme-UV (EUV) range (10 - 120 nm), has a strong effect on the chemical composition of the atmosphere (Chadney et al. 2015). Similar effects are therefore also expected in the atmospheres of exoplanets especially those orbiting M dwarfs which remain active in the EUV much longer than Sun-like G-stars (luminosity factors of 10 - 100 times higher than the solar flux (Ribas et al. 2016)) (Lammer et al. 2011). EUV radiation significantly alters the chemical composition of the upper atmosphere of exoplanets during the early phase of their evolution through interaction with the most abundant molecular species, but its long-term effect on the habitability of planets is complex and remains an open question (Luger & Barnes 2015; Wordsworth & Pierrehumbert 2014; Bolmont et al. 2016; Owen & Mohanty 2016). The thermosphere is a complex chemical environment where the main atmospheric components are dissociated and ionized, leading to efficient ion-molecule reactions involving their primary volatile elements (Moses et al. 2011). Many atmospheric chemical models, adapted mostly to hot exoplanets, are available in the literature, some of which considering the effects of metals and simple ions, like H_3^+, in non-equilibrium models (Muñoz 2007; Helling & Rimmer 2019; Drummond et al. 2016; Yelle 2004; Lavvas et al. 2014; Koskinen et al. 2013; Rimmer & Helling 2016). However, there is no existing study focused on the characterization of the main positive ions that may form within the thermosphere of warm exoplanets and their expected important effects on the chemistry are yet to be quantified. In particular, any effect on the distribution of the IR-radiating species which drive thermal and non-thermal atmospheric escape processes will influence the retention of planetary atmospheres. Determining whether a low-gravity planet around a small active star is able to retain its volatile components is a critical question to understand its nature and evolution. For rocky temperate

planets, in particular, this question is pivotal to understand their potential habitability (Luger & Barnes 2015; Bourrier et al. 2017) since UV irradiation may also stimulate the synthesis of prebiotic molecules (Rimmer et al. 2018).

We are at the dawn of a new era in space exploration with the upcoming launch of new telescopes like the *Atmospheric Remote-Sensing Infrared Exoplanet Large-survey* (ARIEL) (Tinetti et al. 2018) and the *James Webb Space Telescope* (JWST) (Gardner et al. 2006). They will provide a unique insight into the thermal structure and chemical composition of the atmosphere of exoplanets, due to their spectral range and array of instruments that will be used for transmission, emission and phase-curve spectroscopy. To make the most of these future observations, it is important to learn as much as possible about their atmospheric chemistry. Among the different approaches, experimental laboratory simulation is a powerful tool for understanding the chemical evolution of an exoplanet atmosphere and also for guiding observations and the development of atmospheric models. However, so far in the literature, previous laboratory experiments have focused on solid particles (production rates, size, chemical composition) that may constitute photochemical hazes within the cold and warm atmospheres of exoplanets (Hörst et al. 2018; He et al. 2018a,b; Wolters et al. 2019; Moran et al. 2020; Vuitton et al. 2019a).

In order to complete this crucial phase of experimental simulation, it is also necessary to study the chemical evolution of the gas-phase in the primary upper atmosphere of exoplanets following UV irradiation of host stars and to identify the abundant species that may form. While He et al. (2019) studied the neutral species involved in the gas-phase chemistry of simulated exoplanet atmospheres, the implication of the positive ions has never been studied. Photoproducts drive the formation of hazes lower in the atmosphere but are also the starting point for the formation of prebiotic molecules. To be able to detect biosignatures that will be critical to the search for life, this work paves the first milestones with innovative photochemical-driven molecular growth laboratory experiments and shows the direct relationship with space observations.

The approach in this article aims at providing information on chemical species, in particular, charged species that are expected in the thermosphere of rocky and gas-rich exoplanets and could

detectable with future ARIEL and JWST observations. To achieve this goal and to show how the combination of laboratory simulation and numerical modeling constrains the inputs in the modeling of the observations, this work has been divided into three steps:

-In a first step, we have experimentally simulated the effect of UV radiation on simplified gas phase samples (H_2-CO-N_2-H_2O) whose variation of the hydrogen mixing ratio allows us to mimic cases of super-Earths and mini-Neptunes. This first experimental study allowed the measurements of both neutral and cations and to identify the main positive ions formed in H_2-poor and H_2-rich environments.

-In the second step, we analyzed the main pathways of formation of these ions using a photochemical model. The characterization of the photoproducts and the identification of key reactions allowed us to confirm that these experimental results were transposable to planetary environments and that these species could also be formed in significant abundance in the thermosphere of exoplanets.

-In the third step, we carried out simulations of observations using the resolution of the future JWST and ARIEL space telescopes to determine whether it was possible to detect in a transmission spectrum of an exoplanet two of the major ions observed in laboratory experiments with realistic mixing ratios. Due to the lack of chemical information on the atmospheres of exoplanets, we chose a planet whose composition most closely resembles one of the gaseous mixtures used in the laboratory (mini-Neptune GJ1214b) where CO replaced by methane is the only difference, but whose impact on the formation of ions is nil.

2. METHODS

2.1. *Photochemical Reactor Coupled to an EUV Photon Source*

Simplified super-Earth and mini-Neptune atmospheres are reproduced in the laboratory using a photochemical reactor that has already been used in the past for photochemical experiments simulating complex environments similar to the upper layers of planetary atmospheres (Carrasco et al. 2013; Peng et al. 2014; Bourgalais et al. 2019). The cell is filled with a gas mixture representative of the

environments to be reproduced. The species of the gas mixture are then irradiated by an EUV photon source windowless coupled to the photochemical reactor. The energetic particles are produced by a microwave plasma discharge of a rare gas at low pressure providing radiation at different wavelengths depending on the gas used (Tigrine et al. 2016). The chemical species present in the reactor are probed at steady-state using a quadrupole mass spectrometer (*Hiden Analytical EQP 200 QMS*) to measure neutral compounds and positive ions with a high sensitivity below parts-per-million (ppm) level (Bourgalais et al. 2019; Dubois et al. 2019).

In this work, we use a surfatron-type discharge with a neon gas flow that allows us to irradiate the gas mixture of the photochemical cell at an overall pressure of 0.9 mbar and at room temperature. The pressure is adjusted to represent atmospheric pressures of exoplanets but is experimentally constraint in the simulated environments. Reaching the low pressures found in the higher layer of exoplanet environments is not possible due to experimental constraints. The configuration of the device shown in Bourgalais et al. (2019), shows that the inlet of the MS is located very close from the outlet of the VUV lamp in order to limit wall effects and as a consequence the working pressure adjusted to ensure that reactions would take place before detection with the mass spectrometer. The working pressure is barely higher than the pressure (*ca.* 0.01-0.1 mbar) at which EUV radiation penetrates (Lavvas et al. 2014) and is low enough to avoid termolecular effects as in the actual low-density exoplanet thermospheres. Thus, the higher pressure increases the kinetics in the experiments but the results obtained on the chemistry of the ions remain transposable to the atmospheres of exoplanets. The temperature of the thermospheres of exoplanets can reach tens of thousands of Kelvin, whereas our experiments were conducted at room temperature. However, in the lower part of the thermospheres, the deposition of stellar energy can be compensated mainly by the radiative emission of cooling ions and the subsequent ion chemistry, so that the temperature can drop to 1,000 or even a few hundred of Kelvin (Yelle 2004; Koskinen et al. 2007). At these relatively high temperatures, the temperature dependence of the rate coefficients and branching ratios can be very important. Therefore, it should be noted that the temperature dependence of the formation pathways of the main ions highlighted in this work, was studied with a 0D-photochemical model described in

the following section. Numerical simulations performed at room temperature and at 1,000 K, show the same major ions for the two extreme cases discussed in this article. As a conclusion, the simulated environments are relevant to study photochemical mechanisms in upper layer of cold and potentiallly warm exoplanetary atmospheres ($<$ 1,000 K) but these extrapolations at high temperatures must be taken with caution as there is little data on rate coefficients and branching ratios in the literature.

A wavelength of 73.6 nm corresponding to a photon energy of 16.8 eV is used with a flux of about 10^{14} ph cm^{-2} s^{-1} leading to an ionization rate of ca. 10^{-6}. This wavelength is chosen to reach the ionization threshold of the chemical species of the gas mixture that is composed of H_2, CO, and N_2. With this wavelength and the pressure in the reactor, we mimic the stellar EUV field of a star in an upper atmospheric layer (France et al. 2016; Youngblood et al. 2016; Loyd et al. 2016). Transitional planets with a size between Earth and Neptune appear to have a diversity of compositions that is not well-explained but everyone agrees that low-density planets are mainly composed of molecular hydrogen but some super-Earths and mini-Neptunes will likely have thick atmospheres that are not H_2-dominated. Bulk atmospheric composition could have a wide variety of elemental abundance ratios in which the amount of H_2 has profound effects on the evolution of the atmosphere (Pierrehumbert & Gaidos 2011). Our approach is to use gas mixtures containing H_2 along with other expected important molecules in upper layers of cool super-Earth atmospheres. We vary only the relative proportions of H_2 within a large range to test the contribution of H_2 in the formation of photoproducts in the cases of H_2-poor and H_2-rich environments which are representative of simplified super-Earth and mini-Neptune upper atmospheres (Rimmer & Rugheimer 2019). We focus on Earth-like planets by adding N_2 to the gas mixtures (Wordsworth & Pierrehumbert 2014) containing H_2 and since the bulk atmospheric composition of such environment is defined and affected largely in term of the C/O ratio, CO is adding as the only major source of carbon and oxygen to keep a ratio of 1 (Rimmer & Rugheimer 2019). Three gas mixtures have been used with different initial fractional abundances of H_2. The first is a gas mixture at 1% H_2, the second is an intermediate at 33% H_2 and finally the third is a mixture at 96% H_2. The mixing ratio of N_2 was arbitrarily chosen equal to that of CO. Finally, water vapor is the major trace species at ppm level in the reactor coming from residual adsorption

on the reactor walls. Contrary to a previous study on Titan conducted with the same device in Bourgalais et al. (2019), here the reactor was not heated to minimize the presence of residual water and the pressure in the reactor is higher (0.9 mbar in this work versus 0.01 mbar in Bourgalais et al. (2019). Gao et al. (2015) showed that water vapor can have profound effects on the evolution of the planet's atmosphere. Thus, the presence of water vapor traces in the reactor provides a study of the impact of trace level of water vapor in the atmosphere of exoplanets.

Mass spectra reported in this study are the average of 10 scans obtained at 2 s/amu with a channeltron-type detection, over the 1-50 amu mass range. In all the spectra presented below, signals with intensities lower than 1,000 cps are considered as background noise. The reported mass spectra show the direct signal recorded without background subtraction. The duration of the irradiation is only a few minutes because, as the numerical simulations in this manuscript show, the state of equilibrium is reached in less than 1 ms for the main species because their abundance is constant. The stability of the ion signal over the 10 mass spectra recorded during the irradiation supports the claim that the steady state is reached very quickly.

2.2. *0D-Photochemical Model*

To interpret the experimental mass spectra, a coupled ion-neutral photochemical model was used to reproduce the chemistry occurring in the reactor. The model has been detailed in the literature (Peng et al. 2014). We provide here a short description, mentioning the main updates since the initial paper.

2.2.1. *The Reactor Model*

We consider a simplified 1-cell (0D) geometry of the reactor, assuming a uniform spatial distribution of the species. The gas inflow and outflow are taken into account to ensure a constant pressure, and radiative transfer is treated through Beer-Lambert-type photoabsorption, in the assumption of a uniform gas. The chemical reaction are treated as a system of ordinary differential equations (ODEs).

The implicit-explicit Runge-Kutta-Chebyshev (IRKC) method (Shampine et al. 2006) is used to integrate the system of partial differential equations. The photolysis and transport are treated ex-

plicitely (complex evaluation of jacobian elements for radiative-transfer makes it impractical to regard the photolysis rate equations as ordinary differential equations). The chemical ODEs are treated implicitely. The IRKC method handles stiff ODE systems (Verwer & Sommeijer 2004).

The fortran Reactor code is publicly available at https://github.com/ppernot/Reactor, with bash scripts for execution of parallel Monte Carlo runs on an OpenStack cloud (CloudReactor). A graphical interface (ReactorUI) is provided for the analysis of the results.

2.2.2. *Chemistry*

The MC-ChemDB Database—The MC-ChemDB database (MC-ChemDB) has been designed to handle the uncertainty on the rate parameters of chemical reactions (Hébrard et al. 2006, 2009; Carrasco et al. 2008; Plessis et al. 2012) and of photolysis processes (Gans et al. 2010; Peng et al. 2014). The principle is based on a server-client architecture. The server generates and hosts random sets of databases for Monte Carlo uncertainty propagation (BIPM et al. 2008). The client gathers the required number of samples for adapted chemical schemes: depending on the gas mixture in the reactor, only the pertinent subset of the database is used.

The database is split in three modules (neutral reactions, ionic reactions and photolysis) that require different treatments to generate random reaction rate parameters:

- Neutral chemistry (bimolecular thermal reactions and termolecular thermal recombinations) is built from Hébrard et al. (2006, 2009); Dobrijevic et al. (2016). Bimolecular rate constants are represented with the Kooij (modified Arrhenius) rate law, and termolecular association with a pressure-dependent Lindeman-Troe rate law (Dobrijevic et al. 2016; Vuitton et al. 2019b). The scheme is based on partial rate constants.

- Ionic chemistry (ion-molecule reactions and dissociative recombinations) is built from Carrasco et al. (2008); Plessis et al. (2012). Rate laws for ion-neutral reactions are mostly based on the Langevin law, with temperature-dependent laws of type ionpol (Wakelam et al. 2012) for molecules with non-zero dipole moments. Dissociative recombinations are based on a modified Arrhenius rate law (Plessis et al. 2012). The global reaction rates and branching ratios are treated separately.

- Photo-processes (photo-dissociation and photo-ionization), cross-sections and branching ratios (BR)

are extracted from the Leiden database (http://www.strw.leidenuniv.nl/~ewine/photo) (Heays et al. 2017). If BR are not provided by Leiden, they are extracted from SWRI (https://phidrates.space.swri.edu) (Huebner & Mukherjee 2015), except for CH_4, where the representation by Peng et al. (2014) is used. Cross-sections are provided with a 1 nm and 0.1 nm resolutions. At this stage, temperature-dependence of the cross-sections and BRs is ignored.

For a description of the parameters uncertainty representations, see Peng et al. (2014). The database was originally oriented on the chemistry of H, C, and N-bearing species, and it has recently been upgraded to account for oxygenated species from Vuitton et al. (2019b) and the KIDA database (Wakelam et al. 2012).

The photochemical scheme—According to the following procedure a consistent set of reactions is iteratively generated from the irradiated initial mixture (H_2/N_2/CO/H_2O):

1. Select all the reactions involving the list of species;
2. Update the list of species with the generated products;
3. Iterate to (1) until no new species is produced.

The resulting chemical model contains 54 photo-processes (photolysis of N_2, H_2, CH_4, C_2H_2, C_2H_4, C_2H_6, HCN, NH_3, CO & H_2O), 903 neutral reactions (811 bimolecular and 92 termolecular), 1941 ion processes (1314 bimolecular and 687 dissociative recombinations), involving 177 neutral species, 190 positive ions with masses up to 130 and electrons.

Simulations—The model simulates chemistry under conditions similar to those of the experiments (Bourgalais et al. 2019). It is run for a time long enough to reach a stationary state (1 s) and the stationary mole fractions of the products are compared with the experimental data. Complementary Monte Carlo simulations are performed to evaluate the uncertainty on the model predictions (500 runs). A global rate analysis is performed to identify key reactions and dominant formation pathways (Hébrard et al. 2009).

2.3. *Simulations of Observations with ARIEL and JWST*

We investigate the feasibility to detect the ions H_3^+ and H_3O^+ in sub-Neptune type planets using the radiative transfer code TauREx3 (Waldmann et al. 2015b,a). Our approach consists in simulating a high resolution spectrum using TauREx in forward mode. Then we use our instrument simulators ArielRad (Mugnai et al. 2019) to bin down the observations and estimate the instrument noise. As we are investigating the theoretical detection biases through retrieval techniques, we do not scatter the observed spectra (Changeat et al. 2019; Feng et al. 2018). Finally, we retrieve the simulated observations using TauREx3 to check whether the ion signals can be statistically recovered.

We base our simulations on the bulk parameters for GJ1214b from Harpsøe et al. (2013): we use a planet radius of 0.254 R_j, a planet mass of 0.0197 M_j and a star radius of 0.216 R_s. In the case of ARIEL, we consider that all the Tier 3 observations for this planet are stacked together (total of 10 transits) (Tinetti et al. 2016), while for JWST we combine single observations from NIRISS and NIRSpec (total of 2 transits) to roughly match the wavelength coverage. The atmosphere is assumed to be isothermal at 700 K and filled with H_2 and He. We add the trace gases H_2O and CH_4 along with the two ions H_3^+ and H_3O^+. For our simplified model, the abundances for H_2O and CH_4 are set to 10^{-5} and are constant with altitude. For the ions, we base our input abundances on profiles resembling those from Helling & Rimmer (2019). As it is expected for sub-Neptune type planets, we enhance their abundance findings by approximately one order of magnitude and use the 2-layers model (Changeat et al. 2019) to describe the abundance decrease deeper in the atmosphere. For H_3^+, the top abundance is 10^{-5} and the surface abundance is 10^{-14} with a layer pressure change at 10^{-5} bar. For H_3O^+, the top abundance is also 10^{-6} and the surface abundance is 10^{-14}. The layer change is done deeper at 10^{-3} bar. On top of this, we add a grey cloud cover which is fully opaque below 5×10^{-3} bar as expected for this planet (Kreidberg et al. 2014; Kempton et al. 2011; Morley et al. 2013). For the molecular absorptions, we use the most up-to-date molecular line lists from the ExoMol project (Tennyson et al. 2016), HITEMP (Rothman et al. 2010) and HITRAN (Gordon et al. 2016) and build the cross-section tables at a resolution of 10, 000. We also consider absorptions from Rayleigh scattering and Collision Induced Absorption (only the pairs H_2-H_2 and H_2-He). The list of opacities used in this paper is summarised in Table 1.

Table 1. List of IR opacities used in this work.

Species	References
H_2-H_2	(Abel et al. 2011; Fletcher et al. 2018)
H_2-He	(Abel et al. 2012)
H_2O	(Barton et al. 2017; Polyansky et al. 2018)
CH_4	(Hill et al. 2013; Yurchenko et al. 2014)
H_3^+	(Mizus et al. 2017)
H_3O^+	Yurchenko et al. (to be published)

Table 2. List of retrieved parameters and their corresponding uniform prior bounds.

Parameter	Mode	Bounds
Radius	Linear	0.1-0.4 R_j
H_2O	Log	$0.1\text{-}10^{-12}$
CH_4	Log	$0.1\text{-}10^{-12}$
H_3^+	Log	$0.1\text{-}10^{-12}$
H_3O^+	Log	$0.1\text{-}10^{-12}$
Temperature	Linear	300-1500 K
Clouds Pressure	Log	$10\text{-}10^{-7}$ bar

For our retrieval step, the parameter space is explored using the Multinest algorithm (Feroz et al. 2009) with 500 live points and an evidence tolerance of 0.5. The list of retrieved parameters and their corresponding uniform prior bounds are shown in Table 2.

3. RESULTS

3.1. *Identification by mass spectrometry of the neutral species formed in the experiments*

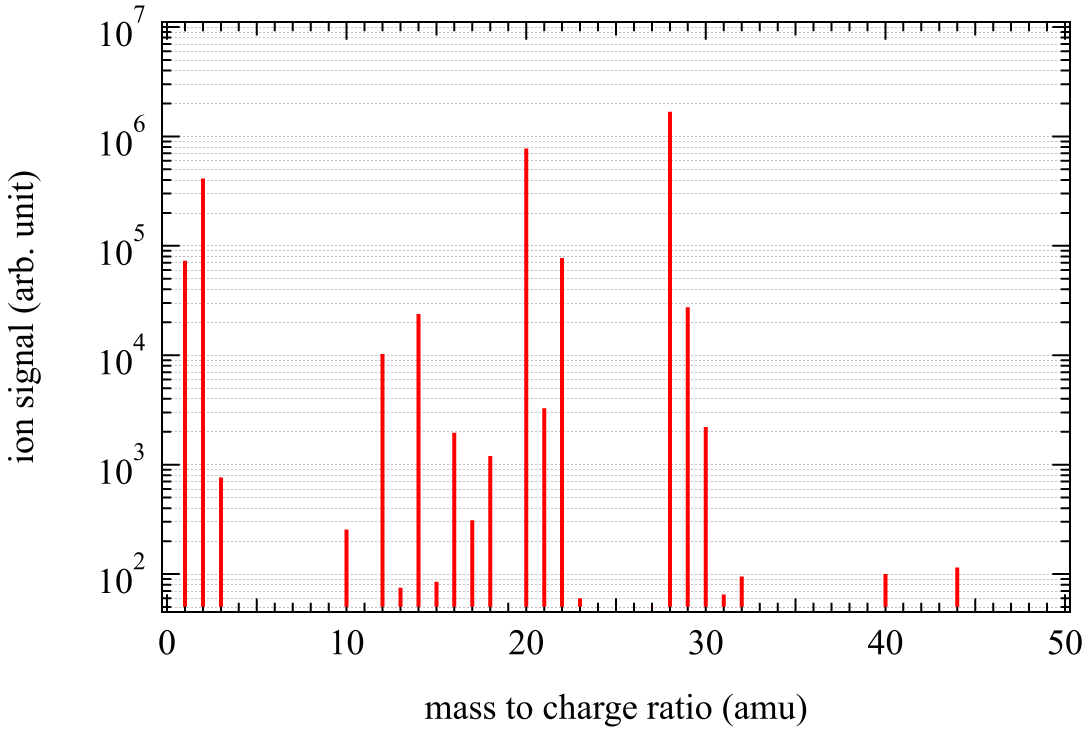

Figure 1. Typical *in situ* gas-phase mass spectrum of neutral species present in the reactor with a H_2-CO-N_2 gas mixture after EUV irradiation.

A typical measured neutral mass spectrum is shown in Figure 1 and displays the abundant peaks of the initial gas mixture species H_2 (m/z = 2), CO and N_2 (both at m/z = 28, with isotopologues at m/z of 29, 30 and 31). Atomic species H, C, N and O resulting from the fragmentation of their parental molecules upon photodissociation are observed at m/z of 1, 12, 14 and 16, respectively. Peaks at m/z of 20, 21 and 22 match the isotope relative abundances of neon, which is the non-reactive gas flowed continuously in the photochemical reactor. Peak at m/z of 10 is attributed to double ionized $^{20}Ne^{2+}$, produced in the mass spectrometer itself by electron impact ionization at 70 eV for the detection of neutral species. Finally, we also observed peaks at m/z of 17 (OH) and 18 (H_2O).

We are conducting our experiments in an open system, where the gas mixture is introduced and pumped continuously. In the reactor, the residence time is short, making it difficult to detect neutral molecules larger than 40 amu. Neutral species beside initial gas mixture contain only atomic species H,

C, N and O resulting from the fragmentation of their parental molecules upon photodissociation, neon which is the non-reactive gas owed continuously in the photochemical reactor and small molecules formed during the first reaction such as CO_2.

Thus, the experimental results obtained for neutral species in this work do not provide as much information and the rest of the study will focus on positive ions, about which our knowledge in this type of environment is much more limited. It should also be noted that the rate of production of ionic products relative to neutral products is similar, with molar fractions of the order of ppm relative to neutral species in the initial gas mixtures.

3.2. *Identification by mass spectrometry of the main ions formed in the experiments*

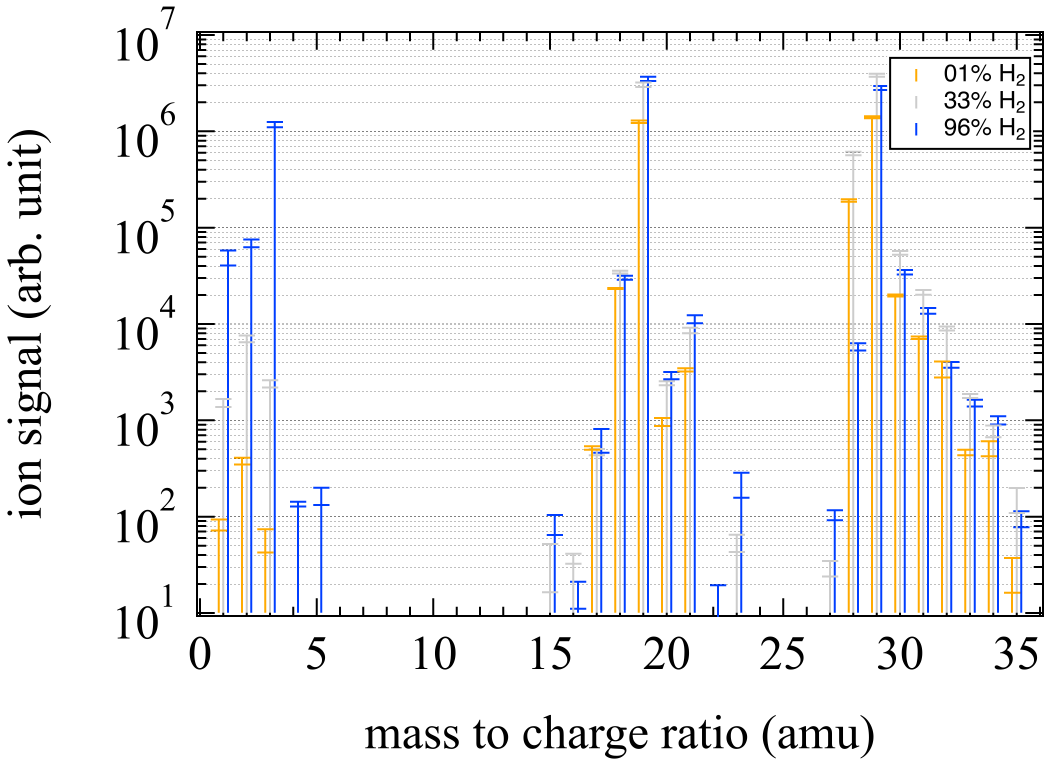

Figure 2. Positive ions measured after irradiation at 73.6 nm of $H_2/CO/N_2$ gas mixtures. H_2 mixing ratios was chosen at 1% (orange), 33% (grey) and 96% (blue) at an overall pressure in the reactor of 0.9 mbar. Twice the standard deviation, 2σ, in 10 measurements of each mass is displayed.

Fig. 2 shows *in situ* non-normalized gas-phase mass spectra of cationic species in their stationary point in the reactor after 15 min EUV irradiation at an overall pressure of 0.9 mbar. The species are detected at *m/z* 1, 2, 3, 18, 19, 20, 21, 28, 29, 30, 31 and 32 above the limit of the background noise. *m/z* 1, 2 and 3 are attributed to H^+, H_2^+, and H_3^+ respectively. Due to the high sensitivity of the mass spectrometer, H_2O^+ and its protonated form H_3O^+ are detected along with first H_3O^+ isotopologues (molecules that only differ in their isotopic composition) at *m/z* 18, 19, 20 and 21. Finally, *m/z* 28, 29, 30, 31 and 32 are attributed to N_2^+ and CO^+, HCO^+ and/or N_2H^+ along with the first HCO^+ isotopologues. The first notable result is that the most abundant ions at *m/z* 19 and *m/z* 29 remain the same with all gas mixtures. The formation of ions H^+, H_2^+, and H_3^+ ions (named H_x ions) does not follow the same trend as the primary ions N_2^+ and CO^+ at mass 28 which are formed by the ionization of N_2 and CO. In the case of H_2-rich gas mixtures, H_x ions, and in particular H_3O^+, dominate while the primary ions N_2^+ and CO^+ occur in significant amounts in the case of gas mixtures where H_2 is not in majority.

3.3. *Unraveling the chemical processes through ion-neutral modelling*

3.3.1. *Hydrogen-poor atmospheres*

Fig. 3 displays the simulated evolution of the mole fractions of the main ionic photo-products after irradiation at 73.6 nm of $H_2/CO/N_2$ gas mixture with a H_2 mixing ratio of 1%. The two most abundant predicted ions using the 0D-photochemical model are HCO^+ and H_3O^+ as observed in the experimental mass spectrum of Fig. 2. The main HCO^+ formation pathways are found to be through the reactions R1, R2, and R3. HOC^+ is formed in a second exit channel of R1 but is rapidly converted into HCO^+ through proton transfer (R3).

$$CO^+ + H_2 \longrightarrow HCO^+/HOC^+ + H \quad \text{(R1)}$$

$$N_2H^+ + CO \longrightarrow HCO^+ + N_2 \quad \text{(R2)}$$

$$HOC^+ + CO \longrightarrow HCO^+ + CO \quad \text{(R3)}$$

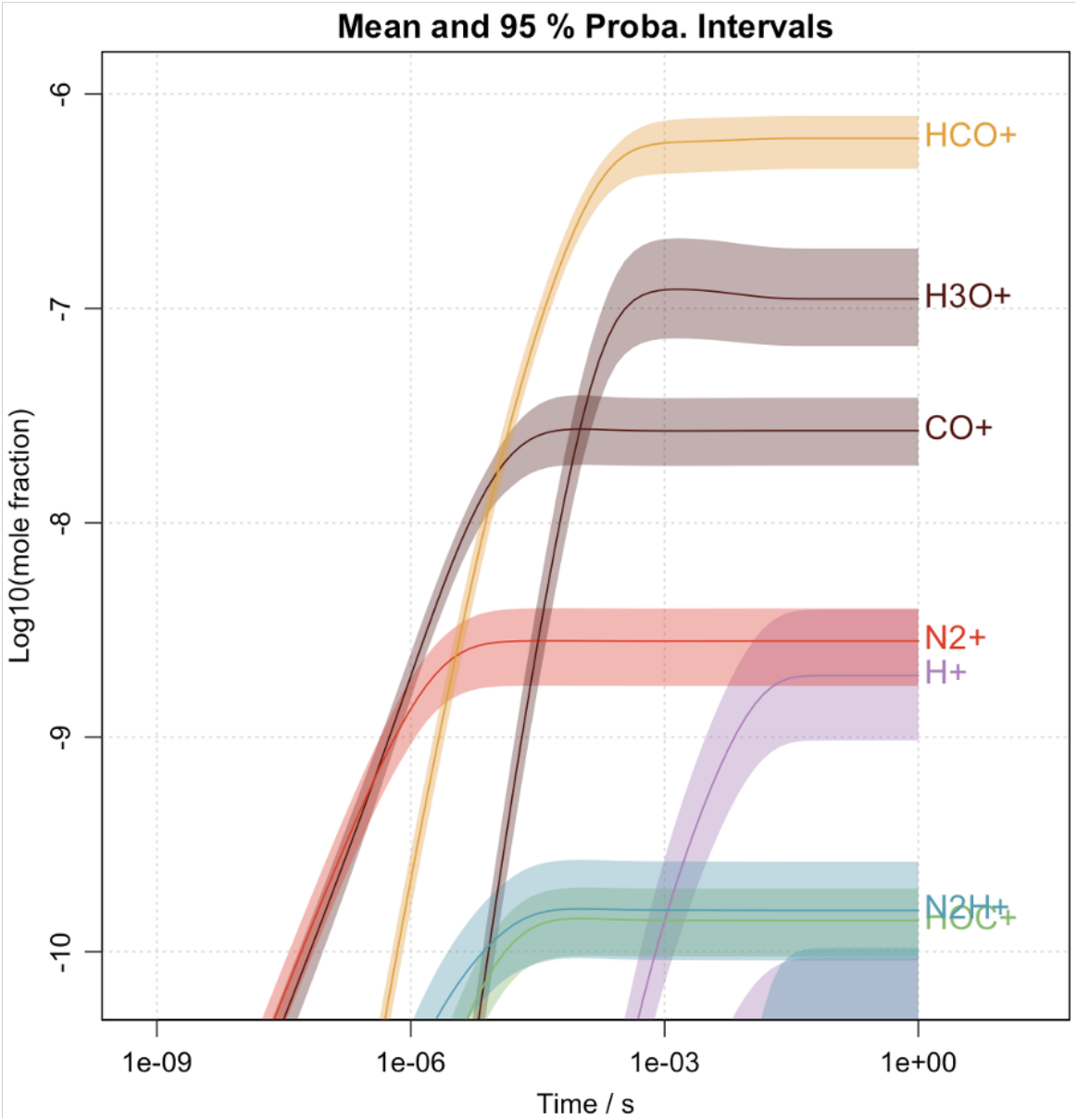

Figure 3. Simulated evolution of the mole fractions of the main ionic photo-products after irradiation at 73.6 nm of $H_2/CO/N_2$ gas mixture with a H_2 mixing ratio of 1%. All species with a mole fraction above 10^{-11} are represented.

The main loss pathways of HCO^+ are found to be dissociative recombination with electrons, along with the proton transfer reaction with water (R4 and R5):

$$HCO^+ + e^- \longrightarrow H + CO \quad \text{(R4)}$$

$$HCO^+ + H_2O \longrightarrow H_3O^+ + CO \quad \text{(R5)}$$

R5 is the only formation pathway for H_3O^+, using trace water vapor in the reactor. H_3O^+ is consumed through dissociative recombination leading to water and OH radicals. Modeling of chemistry within the reactor also shows that the formation of N_2H^+ is negligible compared to that of HCO^+. Its main production pathways are:

$$HOC^+ + N_2 \longrightarrow N_2H^+ + CO \tag{R6}$$

$$N_2{}^+ + H_2 \longrightarrow N_2H^+ + H \tag{R7}$$

The low abundance of N_2H^+ compared to HCO^+ is due to the efficient reaction R2 showing the propensity of CO to consume N_2H^+ to produce HCO^+. As observed in the experimental mass spectrum, the H_x ions are expected to be negligible through the main reactions (R8, R9, and R10).

$$CO^+ + H \longrightarrow H^+ + CO \tag{R8}$$

$$H_2 + h\nu \longrightarrow H_2^+ + e^- \tag{R9}$$

$$HOC^+ + H_2 \longrightarrow H_3^+ + CO \tag{R10}$$

HOC^+ indeed mainly reacts with N_2 and CO (R3 and R6) to produce N_2H^+ and HCO^+ respectively rather than with H_2.

3.3.2. *Hydrogen-rich atmospheres*

Fig. 4 displays the simulated evolution of the mole fractions of the main ionic photo-products after irradiation at 73.6 nm of $H_2/CO/N_2$ gas mixture with a H_2 mixing ratio of 96%. The two most abundant predicted ions using the 0D-photochemical model remain HCO^+ and H_3O^+ as observed in the experimental mass spectrum of Fig. 2. However, the main formation pathways for HCO^+ is still via R3 but with an additional parallel reaction involving H_3^+:

$$H_3^+ + CO \longrightarrow HCO^+ + H_2 \tag{R11}$$

Independent of the mixing ratio of H_2, the main destruction pathways of HCO^+ remain the same in both H_2 environments (R4 and R5) which includes the main production pathway for H_3O^+ (R5).

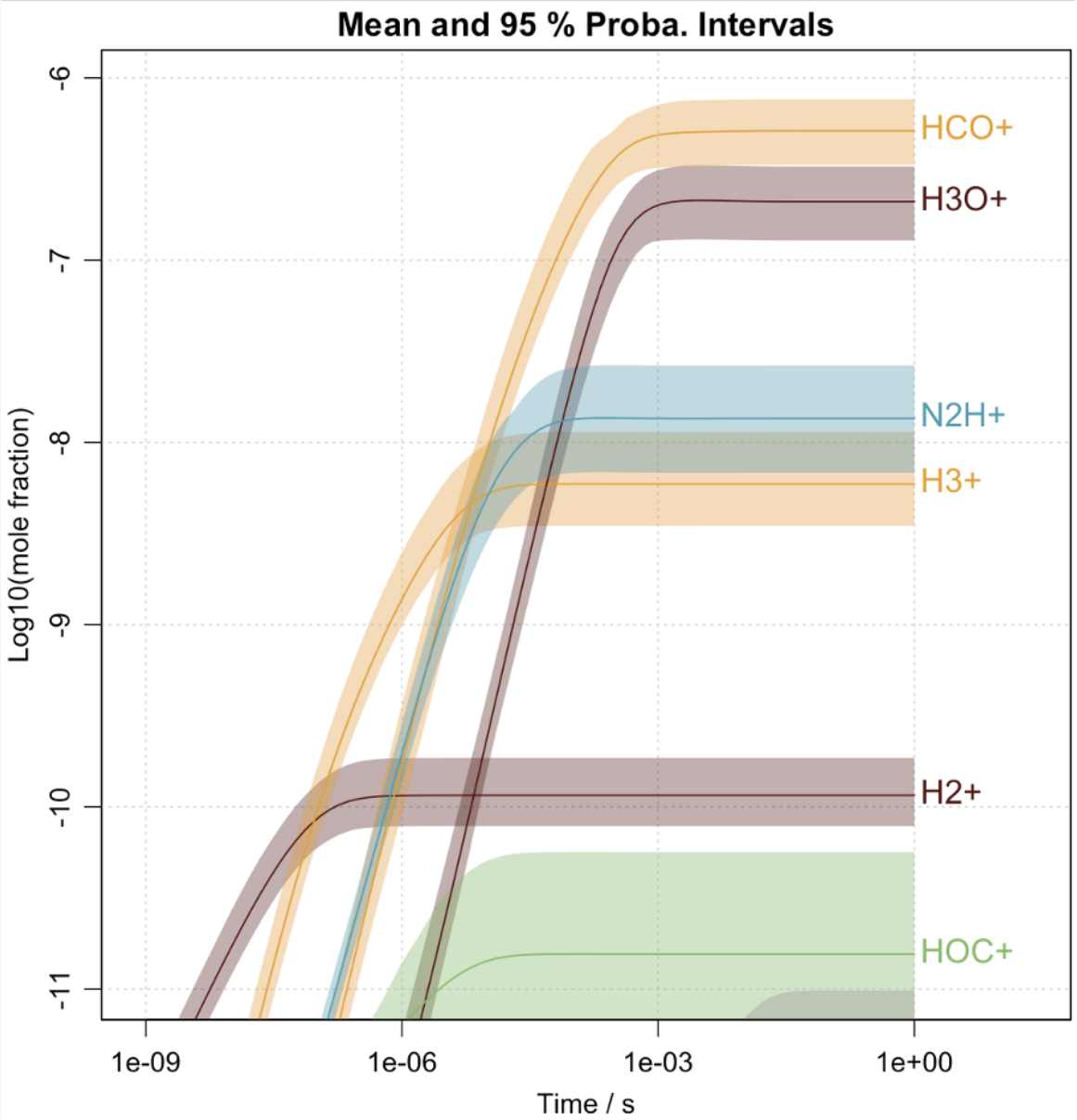

Figure 4. Simulated evolution of the mole fractions of the main ionic photo-products after irradiation at 73.6 nm of $H_2/CO/N_2$ gas mixture with a H_2 mixing ratio of 96%. All species with a mole fraction above 10^{-11} are represented.

Compared to the case of H_2-poor atmospheres, the mole fraction of N_2H^+ increases significantly in the presence of a large abundance of H_2 due to a production pathway more efficient than R6 and R7:

$$H_3^+ + N_2 \longrightarrow N_2H^+ + H_2 \tag{R12}$$

In this H_2-rich environment, H_3^+ starts to be the dominant ion due to a more efficient formation pathway:

$$H_2{}^+ + H_2 \longrightarrow H_3^+ + H \tag{R13}$$

which supersedes R10. Once formed H_3^+ leads to the formation of the dominant ions HCO^+ and N_2H^+ by R11 and R12 respectively.

3.3.3. *Comparison of the two cases*

Laboratory simulations show that the same main ions (HCO^+, H_3O^+) are observed in H_2- poor and rich environments. This implies that we can expect to observe similar contributions of these ions in the thermosphere of super-Earths and mini-Neptunes. However, they are formed through different chemical pathways by H-transfer reactions leading to the observed stable protonated ions. Another remarkable result is that even with trace amounts of water, the formation of the hydronium ion (H_3O^+) is very effective. These results highlight the need to accurately model ion-neutral chemistry in atmospheric models of exoplanets. In the case of the low H_2 environment, the primary ions N_2^+ and CO^+ formed at 73.6 nm trigger the molecular growth reacting with H_2. In the specific case of environments rich in H_2, the triatomic hydrogen ion H_3^+ is one of the most abundant ions and is shown to be very reactive, leading to the formation of heavier ions (N_2H^+ and HCO^+).

3.4. *Simulations of Observations with ARIEL and JWST*

3.4.1. *Choice of the planet type and the ion targets*

The fact that the H_3^+ ion is predicted to be abundant and highly reactive leading to the formation of heavier ions in H_2-rich environments is of great interest in the context of exoplanetary observations considering the upcoming launches of the ARIEL and JWST telescopes. The abundance and distribution of H_3^+, the stable ionic form of H_2 is essential to understand the chemistry and to get information about the thermal structure, the dynamic, and the energy balance of exoplanet atmospheres (Miller et al. 2000). H_3^+ has been thoroughly studied in the mid-InfraRed (IR) on Jupiter (Stallard et al. 2001), Saturn (Geballe et al. 1993) and Uranus (Trafton et al. 1993) but detection in

the thermosphere of hot Jupiter exoplanets, with a predicted mixing ratio ranging from 10^{-6} up to 10^{-4}, so far remains illusive (Lenz et al. 2016; Shkolnik et al. 2006). Helling & Rimmer (2019) assume that the formation pathway of H_3^+ through the ionization of H_2 (R11), although very efficient, is difficult in hot exoplanet atmospheres due to the thermal decomposition of H_2 which becomes important when temperature reaches 1,000 K (Yelle 2004). Indeed, the very hot thermosphere of these exoplanets (> 8,000 K) combined with very intense stellar irradiations promotes the formation of atomic neutral and H^+ making the detection of H_3^+ difficult (Koskinen et al. 2010). However, H_3^+ is an efficient coolant up to 10,000 K, temperature above which thermal dissociation becomes significant and this thermostat effect is important in controlling the atmospheric stability of giant exoplanets (Neale et al. 1996; Miller et al. 2010, 2013). By lowering the temperature of the exosphere and the related pressure, H_3^+ helps to counteract the atmospheric escape of atomic and molecular species. Theory predicts that the cooling potential of H_3^+ would allow one to observe H_3^+ in giant exoplanets inside 0.2 to 1 AU orbits (Yelle 2004; Miller et al. 2013; Koskinen et al. 2007). H_3^+ is able to offset the increased heating due to EUV radiation which allows to produce increased ion densities by photoionization. Thus, to get sufficient H_3^+ an atmosphere relatively cold or far-enough from its star to have a low-temperature thermosphere is needed. The results of the laboratory experiments in this work suggest that colder atmospheres dominated by H_2 would be more conducive to H_2 stability leading to a higher H_3^+ abundance. Warm Neptunes (ca. 400 to 800 K) would therefore potentially be better candidates than hot Jupiters for the detection of H_3^+.

Like H_3^+, long lifetimes associated with certain excited states can lead to population trapping and unexpected state distributions in non-thermalized environments. A recent theoretical study by Melnikov et al. (2016) calculated the stability of the ro-vibrational states of H_3O^+, the lifetimes of individual states and the overall cooling rates. H_3O^+ is present in abundance in diffuse and dense regions of the interstellar medium, such as comets and molecular clouds (Goicoechea & Cernicharo 2001; Barber et al. 2009). So far, no attempt has been made to observe H_3O^+ in the thermosphere of exoplanets, although it may, like H_3^+, act as a cooling agent and bring some constraints on the physical parameters of the atmosphere.

3.4.2. *Simulation of the observation of ions in a GJ1214b-like planet by ARIEL and JWST*

In order to evaluate the ability of future telescopes to detect these two ions, we simulate a simplified atmosphere for a GJ1214b-type warm Neptune planet as observed by JWST and ARIEL with respectively 2 and 10 stacked transits. The chemical profiles we use for the H_3^+ and H_3O^+ ions are inspired by the work of Helling & Rimmer (2019); we also include the absorption of H_2O and CH_4, which are the main absorbers. For our simplified model, the abundances for water vapor and methane are set to 10 ppm and are constant with altitude. Those two molecules are predicted to be abundant in sub-Neptune planets (Kempton et al. 2011; Venot et al. 2014; Hu 2015; Tinetti et al. 2018; Changeat et al. 2019) and have very strong features in the wavelength range covered by Ariel and JWST. As there are still few models of exoplanets to incorporate reactions with ions, the abundances of H_3^+ and H_3O^+ that can be expected remain unclear. We present the results with realistic mixing ratios inspired by the work of Helling & Rimmer (2019) though. The purpose of these simulations was to determine with the resolution of future telescopes if these mixing ratios would allow the cations to be detected in the atmospheres of exoplanets and through which transitions. While their profiles may variate with altitude, for the purpose of our simplified example we consider that they are vertically mixed, hence constant with altitude (see Fig.5).

It should be noted that no object exactly similar to our experimental gas mixtures has yet been identified, but the fact that CH_4 replaces CO/N_2 among the secondary species does not change the final result, which is that H_3O^+ and H_3^+ will be among the major ions formed in a H_2-dominated environment where there is the presence of oxygen, even if only in trace amounts (Hollenbach et al. 2012; Beuther et al. 2014; Gerin et al. 2016). Efficient series of proton transfer reactions from H_3^+ or other abundant ions, depending on the secondary species in the environments, will easily lead to the formation of H_3O^+ (Indriolo & McCall 2013; Van Dishoeck et al. 2013), making the detection of H_3O^+ and H_3^+ in an object like GJ1214b quite legitimate.

In both ARIEL and JWST cases, our retrieval analysis manages to reproduce the observed spectra (see Fig. 6). We can see that H_3O^+ is detectable by both instruments (see also posterior distributions Fig. 7). Indeed, H_3O^+ presents a wide feature around 2.8 μm, which is easily captured. H_3^+, however,

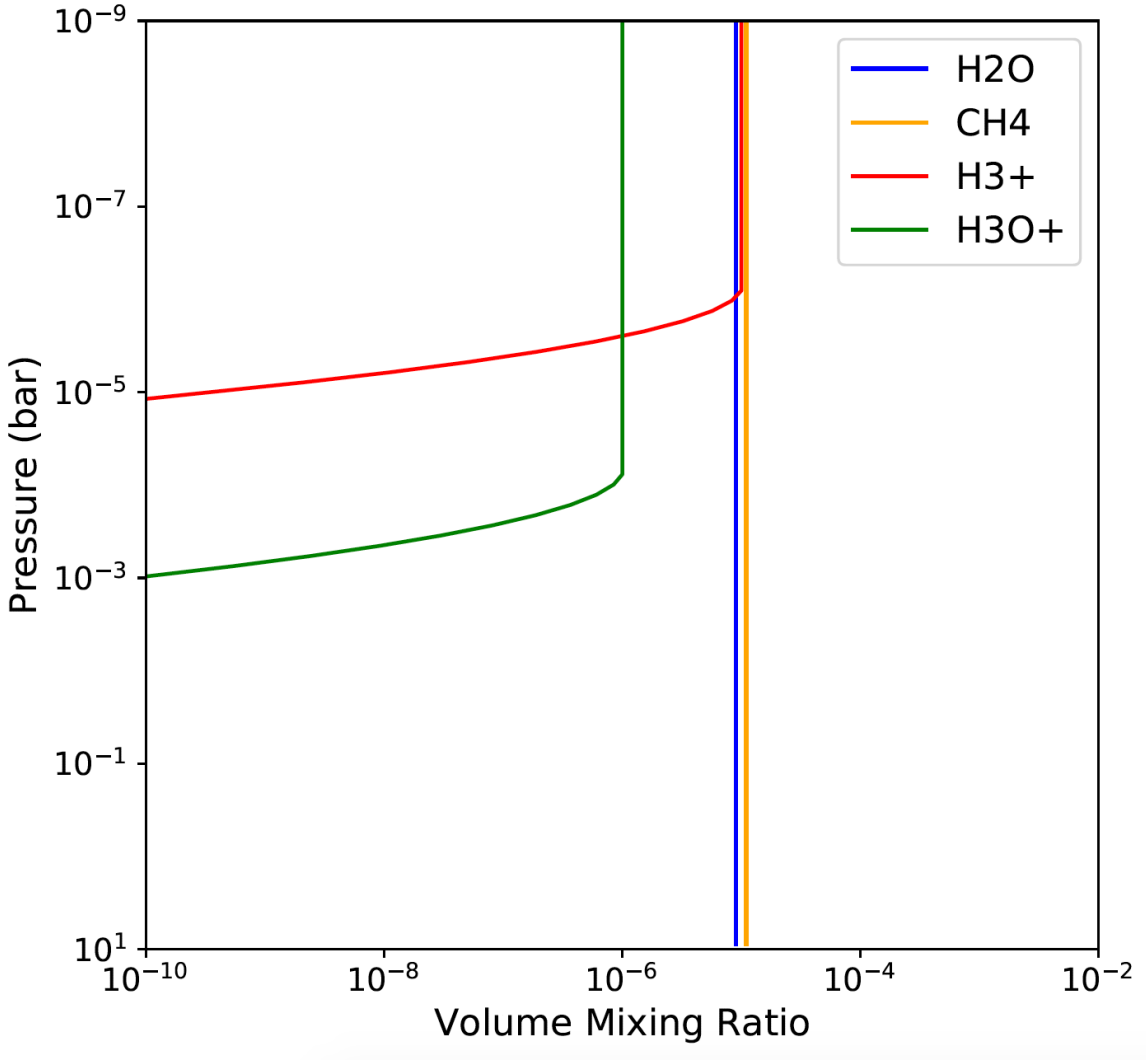

Figure 5. Atmospheric profiles used as input for foward simulations of exoplanet spectrum, as well as for fitting data in retrievals.

exhibits much weaker features that are largely masked by the clouds. In general, the grey cloud cover, which represents a pessimistic assumption, introduces a large degeneracy with the planet radius and the retrieved abundances (see Fig. 8). This, along with the assumption of constant chemistry in the retrievals, explain the slight difference from the true and retrieved chemistry for H_2O and CH_4. H_3^+ is only successfully detected in the JWST simulated spectrum thanks to the presence of small features, only seen at high resolution. In the ARIEL case, an upper limit of 10^{-5} on H_3^+ abundance can be deduced but the detection remains unclear. In order to detect this ion with ARIEL, higher abundances or a slightly higher number of transits will be necessary.

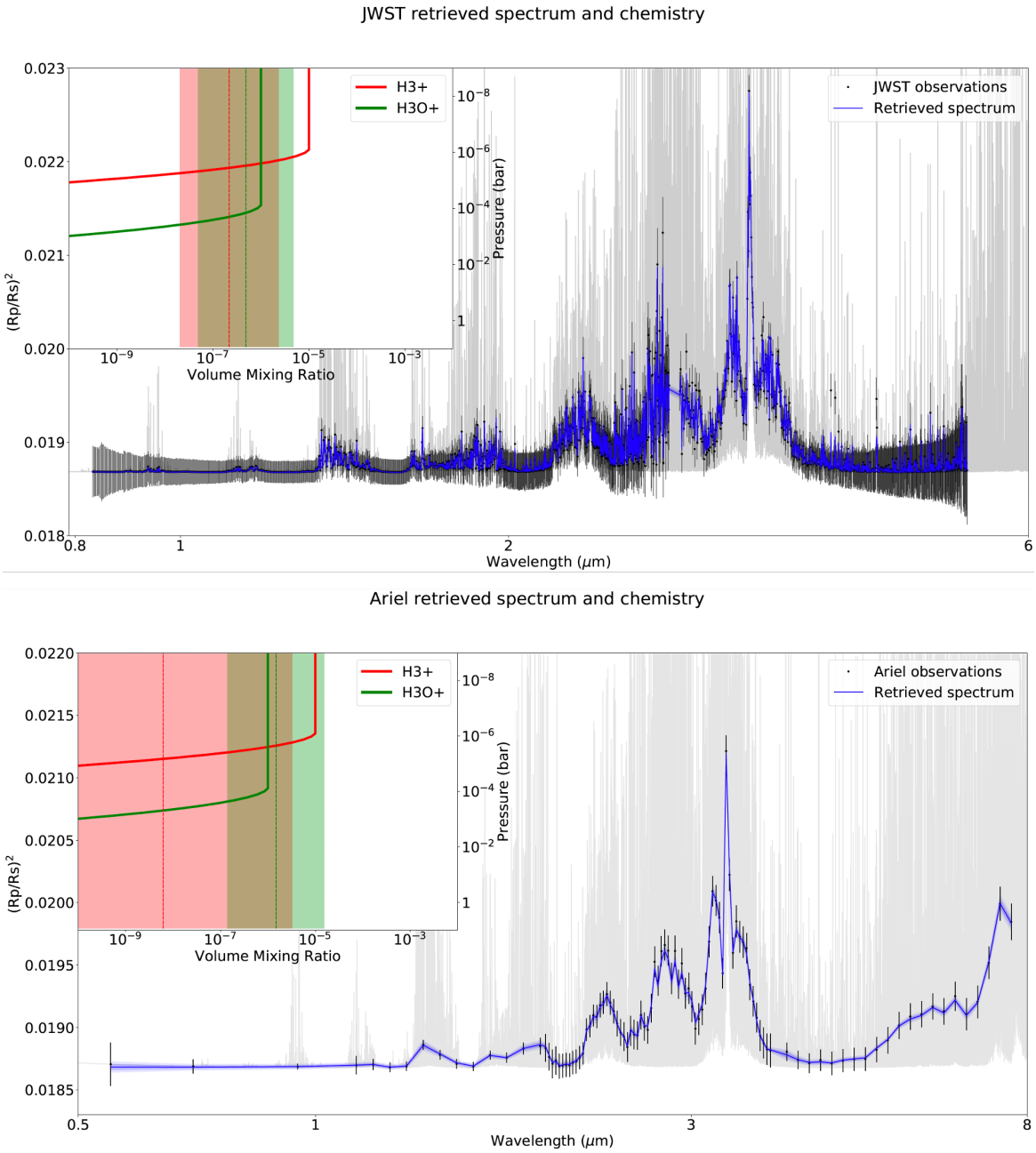

Figure 6. Retrieved spectra and volume mixing ratios for our JWST (top) and ARIEL (bottom) simulations of a GJ1214b-like planet with H_3O^+ and H_3^+ ions. For the abundances the solid line is the true value, the dashed line the mean retrieved value and the shaded area represents the 1σ retrieved value.

4. CONCLUSION

Laboratory experiments simulating thermospheric chemistry in simplified atmospheres of super-Earth and mini-Neptunes exoplanets were performed. A photochemical reactor containing gas mix-

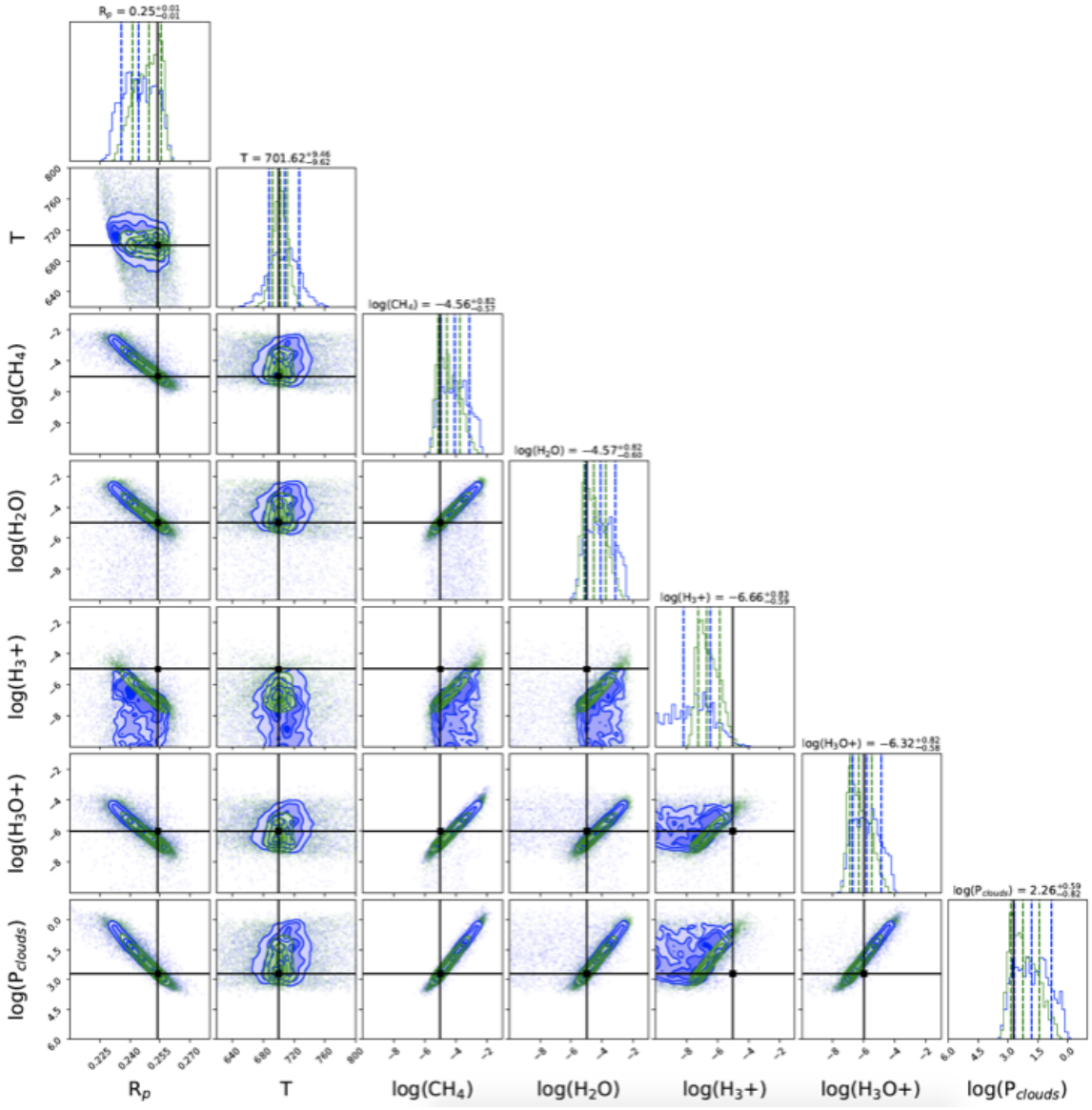

Figure 7. Posterior distributions for ARIEL (blue) and JWST (green) retrievals of our GJ1214b planet case.

tures with different mixing ratios of H_2 and important exoplanetary trace compounds (CO and N_2) were irradiated at a pressure of 0.9 mbar, representative of high altitude in an exoplanetary atmosphere, and a wavelength of 73.6 nm. The photoproduced ions were measured using a quadrupole mass spectrometer and the experimental data were compared to the expected abundances of a 0D-photochemical model. A sensitivity analysis based on the Monte Carlo method allows us to confirm H_3^+ as one of the main ions in environments rich in H_2. Our retrieval analysis based on these sim-

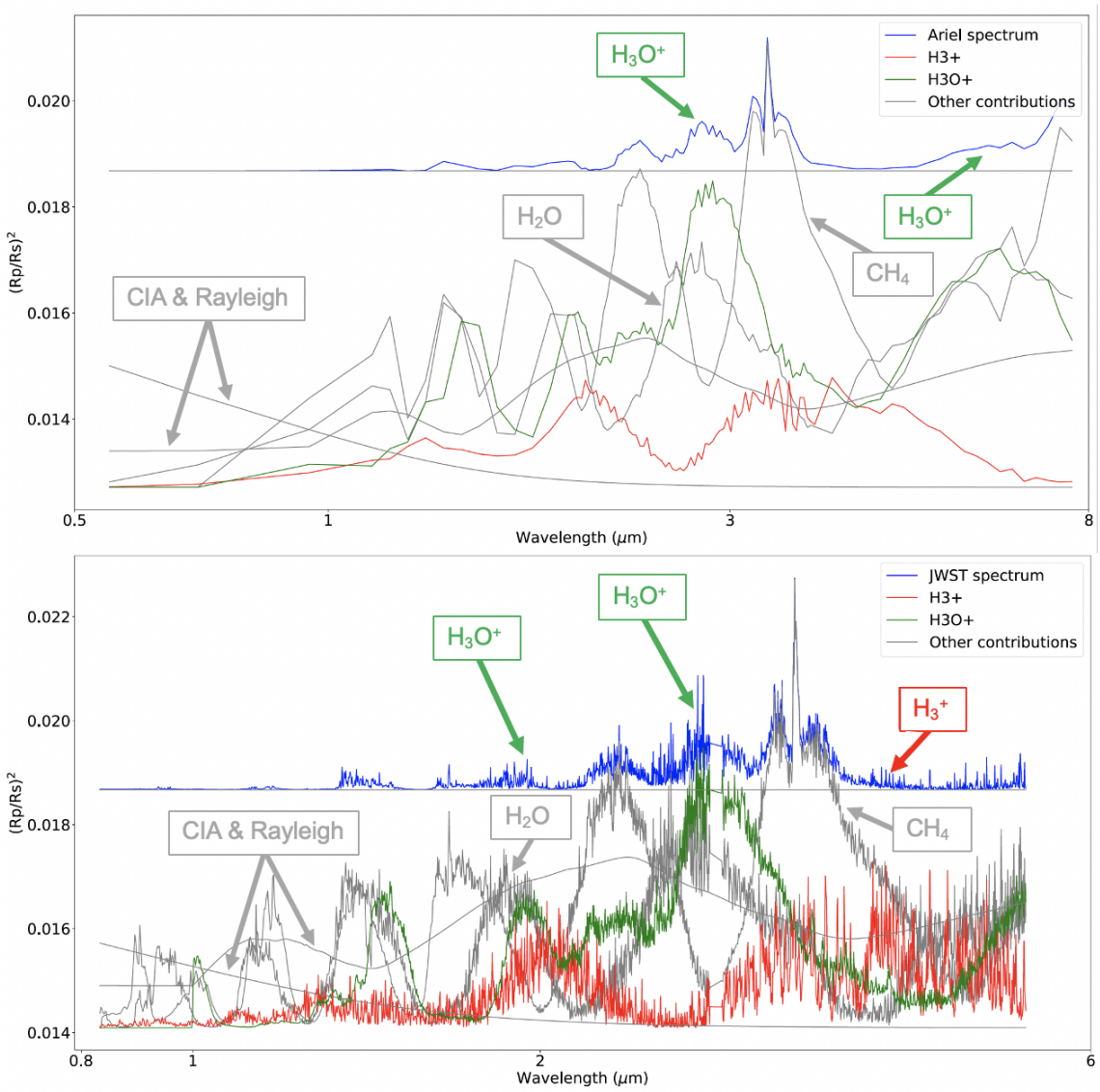

Figure 8. Contribution of the different absorbers to the transmission spectra of our best fit retrievals for ARIEL (top) and JWST (bottom).

ulations show that in realistic conditions, the next generation of space telescopes should be able to accurately constrain H_3O^+ abundances in sub-Neptunes due to the large broadband feature at around 2.8 μm. For H_3^+, the strongest features seem to require high resolution, which can easily be achieved by JWST but would require the stacking of a large number of observations in the case of ARIEL. Even if the presence of other molecules make detections more difficult, spectral retrieval models provide a powerful technique to disentangle the contribution of the different species from

the data (Lammer et al. 2019; Lavie et al. 2017; Goyal et al. 2017; Gandhi & Madhusudhan 2017). Additionally, H_3^+ is very reactive and tends to donate a proton to all the molecules it encounters, enriching chemistry through chain reactions to form more complex and diverse molecules. H_3^+ will thus be difficult to observe if it reacts very quickly with neighboring molecules such as CO and N_2, as shown in this work. Given the results of this work, we suggest that it should be fruitful to search upper exoplanetary atmospheres for abundant protonated ions such as H_3O^+ produced by reactions with H_3^+. The simultaneous detection of H_3^+ and H_3O^+ ions would serve to constrain parameters when characterizing exoplanets.

Several future ground-based and space telescopes (JWST, ARIEL, E-ELT, TMT) will allow the characterization of the atmospheres of exoplanets using infrared spectroscopy, in particular to search for biosignatures within the atmospheres of rocky planets. Cool stars such as M dwarfs are preferred targets for the search of rocky temperate planets, as they have a closer habitable zone due to their size and temperature, which favors the detection and characterization of terrestrial exoplanets (Tarter et al. 2007; Scalo et al. 2007). However, the exposure of planetary atmospheres to the strong UV radiation from these active stars may have drastically negative effect on the habitability of planets (Luger & Barnes 2015; Tian 2009; Erkaev et al. 2013; Miguel et al. 2014; Chadney et al. 2016). High-energy radiation drives the chemical composition, including the formation of IR-radiating species that will influence the evolution of the atmosphere by controlling its thermal structure. Species like H_3^+ and H_3O^+ with different cooling rates will allow different EUV-response to thermospheric expansion and hinder the escape of atoms and other volatiles that could be required for life. Thus, the detection of these ions can provide information on the physical parameters of atmospheres and the formation of atmospheric constituents. For instance the saturated molecular hydronium ion is known to play an important role in planetary and interstellar oxygen chemistry network in a way that dissociative recombination of hydronium ions with electrons could be a source of target molecules related to habitability like water vapor and O_2 (Larsson & Orel 2008). Thus H_3^+ or H_3O^+ may be used to estimate water vapor and O_2 abundances when direct detection is unfeasible.

As a conclusion, this work proposed H_3^+ and H_3O^+ as potential tracers of the nature and evolution of low-gravity exoplanets. H_3^+ formation is negligible in low H_2 environments but important in H_2-rich gas mixtures, while H_3O^+ should remain abundant in both environments if water vapor is present in the atmosphere even at trace level. Thus, non-detection of H_3^+ associated with the observation of H_3O^+ in an exoplanetary atmosphere would provide additional information for the classification of planets in the transition between super-Earths and mini-Neptunes.

Future studies should focus on the potential detection of the other major ions highlighted in this work, HCO^+ and N_2H^+, which may be relatively abundant within the atmospheres of exoplanets where CO and N_2 would be present. However, theoretical calculations are required to provide a list of absorption transitions and their related intensities for these species. One strategy to support the theoretical calculations would be to develop experimental devices to measure ion absorption cross sections in IR. Experimental devices must begin to focus on the evolution of thermospheric chemistry as a function of temperature, which requires the development of simulation chambers that can be temperature-controlled between 300 and 1,000 K. Finally, photochemical models of exoplanets should begin to take into account the coupling between the chemistry of neutral species and ions for the simulation of atmospheres of cold and warm exoplanets.

ACKNOWLEDGMENTS

This research was supported by the European Research Council Starting Grant PRIMCHEM 636829 to N.C.. O.V. thanks the CNRS/INSU Programme National de Planétologie (PNP) and the CNES for funding support. We acknowledge the help and the fruitful discussions with Dr Billy Edwards, who provided access to his JWST noise simulator ExoWebb.

REFERENCES

Abel, M., Frommhold, L., Li, X., & Hunt, K. L. 2011, The Journal of Physical Chemistry A, 115, 6805

—. 2012, The Journal of chemical physics, 136, 044319

Barber, R. J., Miller, S., Dello Russo, N., et al. 2009, Monthly Notices of the Royal Astronomical Society, 398, 1593

Barton, E. J., Hill, C., Yurchenko, S. N., et al. 2017, Journal of Quantitative Spectroscopy and Radiative Transfer, 187, 453

Beuther, H., Klessen, R. S., Dullemond, C. P., & Henning, T. K. 2014, Protostars and planets VI (University of Arizona Press)

BIPM, IEC, IFCC, et al. 2008, Evaluation of measurement data - Supplement 1 to the "Guide to the expression of uncertainty in measurement" - Propagation of distributions using a Monte Carlo method, Tech. Rep. 101:2008, Joint Committee for Guides in Metrology, JCGM. http://www.bipm.org/utils/common/documents/jcgm/JCGM_101_2008_E.pdf

Bolmont, E., Selsis, F., Owen, J. E., et al. 2016, Monthly Notices of the Royal Astronomical Society, 464, 3728

Borucki, W. J. 2016, Reports on Progress in Physics, 79, 036901, doi: 10.1088/0034-4885/79/3/036901

Bourgalais, J., Carrasco, N., Vettier, L., & Pernot, P. 2019, Journal of Geophysical Research: Space Physics, 124, 9214

Bourrier, V., Ehrenreich, D., Wheatley, P., et al. 2017, Astronomy & Astrophysics, 599, L3

Carrasco, N., Alcaraz, C., Dutuit, O., et al. 2008, Planetary and Space Science, 56, 1644

Carrasco, N., Giuliani, A., Correia, J.-J., & Cernogora, G. 2013, Journal of synchrotron radiation, 20, 587

Chabrier, G. 2003, Publications of the Astronomical Society of the Pacific, 115, 763

Chadney, J., Galand, M., Koskinen, T., et al. 2016, Astronomy & Astrophysics, 587, A87

Chadney, J., Galand, M., Unruh, Y., Koskinen, T., & Sanz-Forcada, J. 2015, Icarus, 250, 357

Changeat, Q., Edwards, B., Waldmann, I., & Tinetti, G. 2019, The Astrophysical Journal, 886, 39

Coughlin, J. L., Mullally, F., Thompson, S. E., et al. 2016, The Astrophysical Journal Supplement Series, 224, 12

Dobrijevic, M., Loison, J., Hickson, K., & Gronoff, G. 2016, Icarus, 268, 313

Drummond, B., Tremblin, P., Baraffe, I., et al. 2016, Astronomy & Astrophysics, 594, A69

Dubois, D., Carrasco, N., Petrucciani, M., et al. 2019, Icarus, 317, 182

Elkins-Tanton, L. T., & Seager, S. 2008, The Astrophysical Journal, 685, 1237

Erkaev, N. V., Lammer, H., Odert, P., et al. 2013, Astrobiology, 13, 1011

Feng, Y. K., Robinson, T. D., Fortney, J. J., et al. 2018, The Astronomical Journal, 155, 200

Feroz, F., Gair, J. R., Hobson, M. P., & Porter, E. K. 2009, Classical and Quantum Gravity, 26, 215003

Fletcher, L. N., Gustafsson, M., & Orton, G. S. 2018, The Astrophysical Journal Supplement Series, 235, 24

France, K., Loyd, R. P., Youngblood, A., et al. 2016, The Astrophysical Journal, 820, 89

Gandhi, S., & Madhusudhan, N. 2017, Monthly Notices of the Royal Astronomical Society, 474, 271

Gans, B., Mendes, L. A. V., Boyé-Péronne, S., et al. 2010, The Journal of Physical Chemistry A, 114, 3237

Gao, P., Hu, R., Robinson, T. D., Li, C., & Yung, Y. L. 2015, The Astrophysical Journal, 806, 249

Gardner, J. P., Mather, J. C., Clampin, M., et al. 2006, Space Science Reviews, 123, 485

Geballe, T., Jagod, M.-F., & Oka, T. 1993, The Astrophysical Journal, 408, L109

Gerin, M., Neufeld, D. A., & Goicoechea, J. R. 2016, Annual Review of Astronomy and Astrophysics, 54, 181

Goicoechea, J. R., & Cernicharo, J. 2001, The Astrophysical Journal Letters, 554, L213

Gordon, I., Rothman, L. S., Wilzewski, J. S., et al. 2016, in AAS/Division for Planetary Sciences Meeting Abstracts# 48, Vol. 48

Goyal, J. M., Mayne, N., Sing, D. K., et al. 2017, Monthly Notices of the Royal Astronomical Society, 474, 5158

Harpsøe, K. B. W., Hardis, S., Hinse, T., et al. 2013, Astronomy & Astrophysics, 549, A10

He, C., Hörst, S. M., Lewis, N. K., et al. 2018a, The Astrophysical Journal Letters, 856, L3

—. 2018b, The Astronomical Journal, 156, 38

He, C., HÃűrst, S. M., Lewis, N. K., et al. 2019, ACS Earth and Space Chemistry, 3, 39

Heays, A., Bosman, AD, v., & Van Dishoeck, E. 2017, Astronomy & Astrophysics, 602, A105

Hébrard, E., Dobrijevic, M., Bénilan, Y., & Raulin, F. 2006, Journal of Photochemistry and Photobiology C: Photochemistry Reviews, 7, 211

Hébrard, E., Dobrijevic, M., Pernot, P., et al. 2009, The Journal of Physical Chemistry A, 113, 11227

Helling, C., & Rimmer, P. B. 2019, arXiv preprint arXiv:1903.04565

Hill, C., Yurchenko, S. N., & Tennyson, J. 2013, Icarus, 226, 1673

Hollenbach, D., Kaufman, M., Neufeld, D., Wolfire, M., & Goicoechea, J. 2012, The Astrophysical Journal, 754, 105

Hörst, S. M. 2017, Journal of Geophysical Research: Planets, 122, 432

Hörst, S. M., He, C., Lewis, N. K., et al. 2018, Nature Astronomy, 2, 303

Hu, R. 2015, in Planetary Exploration and Science: Recent Results and Advances (Springer), 291–308

Hu, R., & Seager, S. 2014, The Astrophysical Journal, 784, 63

Huebner, W., & Mukherjee, J. 2015, Planetary and Space Science, 106, 11

Indriolo, N., & McCall, B. J. 2013, Chemical Society Reviews, 42, 7763

Jontof-Hutter, D. 2019, Annual Review of Earth and Planetary Sciences, 47, 141

Kempton, E. M.-R., Zahnle, K., & Fortney, J. J. 2011, The Astrophysical Journal, 745, 3

Koskinen, T., Aylward, A., Smith, C., & Miller, S. 2007, The Astrophysical Journal, 661, 515

Koskinen, T., Harris, M., Yelle, R., & Lavvas, P. 2013, Icarus, 226, 1678

Koskinen, T., Yelle, R., Lavvas, P., & Lewis, N. 2010, The Astrophysical Journal, 723, 116

Kreidberg, L., Bean, J. L., Désert, J.-M., et al. 2014, Nature, 505, 69

Lammer, H., Sproß, L., Grenfell, J. L., et al. 2019, arXiv preprint arXiv:1904.11716

Lammer, H., Eybl, V., Kislyakova, K., et al. 2011, Astrophysics and Space Science, 335, 39

Larsson, M., & Orel, A. E. 2008, Dissociative recombination of molecular ions (Cambridge University Press Cambridge)

Laughlin, G., Bodenheimer, P., & Adams, F. C. 2004, The Astrophysical Journal Letters, 612, L73

Lavie, B., Mendonça, J. M., Mordasini, C., et al. 2017, The Astronomical Journal, 154, 91

Lavvas, P., Koskinen, T., & Yelle, R. V. 2014, The Astrophysical Journal, 796, 15

Lenz, L., Reiners, A., Seifahrt, A., & Käufl, H.-U. 2016, Astronomy & Astrophysics, 589, A99

Loyd, R. P., France, K., Youngblood, A., et al. 2016, The Astrophysical Journal, 824, 102

Luger, R., & Barnes, R. 2015, Astrobiology, 15, 119

Melnikov, V. V., Yurchenko, S. N., Tennyson, J., & Jensen, P. 2016, Physical Chemistry Chemical Physics, 18, 26268

Miguel, Y., Kaltenegger, L., Linsky, J. L., & Rugheimer, S. 2014, Monthly Notices of the Royal Astronomical Society, 446, 345

Miller, S., Stallard, T., Melin, H., & Tennyson, J. 2010, Faraday discussions, 147, 283

Miller, S., Stallard, T., Tennyson, J., & Melin, H. 2013, The Journal of Physical Chemistry A, 117, 9770

Miller, S., Rego, D., Achilleos, N., et al. 2000, Advances in Space Research, 26, 1477

Mizus, I. I., Alijah, A., Zobov, N. F., et al. 2017, Monthly Notices of the Royal Astronomical Society, 468, 1717

Moran, S., Horst, S., Vuitton, V., et al. 2020, AAS, 52, 248

Morley, C. V., Fortney, J. J., Kempton, E. M.-R., et al. 2013, The Astrophysical Journal, 775, 33

Moses, J. I., Visscher, C., Fortney, J. J., et al. 2011, The Astrophysical Journal, 737, 15

Moses, J. I., Line, M. R., Visscher, C., et al. 2013, The Astrophysical Journal, 777, 34

Mugnai, L., Edwards, B., Papageorgiou, A., Pascale, E., & Sarkar, S. 2019, EPSC-DPS Joint Meeting 2019, 13

Muñoz, A. G. 2007, Planetary and Space Science, 55, 1426

Neale, L., Miller, S., & Tennyson, J. 1996, The Astrophysical Journal, 464, 516

Owen, J. E., & Mohanty, S. 2016, Monthly Notices of the Royal Astronomical Society, 459, 4088

Peng, Z., Carrasco, N., & Pernot, P. 2014, GeoResJ, 1, 33

Pierrehumbert, R., & Gaidos, E. 2011, The Astrophysical Journal Letters, 734, L13

Plessis, S., Carrasco, N., Dobrijevic, M., & Pernot, P. 2012, Icarus, 219, 254

Polyansky, O. L., Kyuberis, A. A., Zobov, N. F., et al. 2018, Monthly Notices of the Royal Astronomical Society, 480, 2597

Ribas, I., Bolmont, E., Selsis, F., et al. 2016, Astronomy & Astrophysics, 596, A111

Rimmer, P. B., & Helling, C. 2016, The Astrophysical Journal Supplement Series, 224, 9

Rimmer, P. B., & Rugheimer, S. 2019, Icarus, 329, 124

Rimmer, P. B., Xu, J., Thompson, S. J., et al. 2018, Science advances, 4, eaar3302

Rothman, L. S., Gordon, I. E., Barber, R. J., et al. 2010, J. Quant. Spectrosc. Radiat. Transf., 111, 2139

Scalo, J., Kaltenegger, L., Segura, A., et al. 2007, Astrobiology, 7, 85

Schaefer, L., Lodders, K., & Fegley, B. 2012, The Astrophysical Journal, 755, 41

Shampine, L. F., Sommeijer, B. P., & Verwer, J. G. 2006, Journal of computational and applied mathematics, 196, 485

Shkolnik, E., Gaidos, E., & Moskovitz, N. 2006, The Astronomical Journal, 132, 1267

Shkolnik, E. L., & Barman, T. S. 2014, The Astronomical Journal, 148, 64

Stallard, T., Miller, S., Millward, G., & Joseph, R. D. 2001, Icarus, 154, 475

Tarter, J. C., Backus, P. R., Mancinelli, R. L., et al. 2007, Astrobiology, 7, 30

Tennyson, J., Yurchenko, S. N., Al-Refaie, A. F., et al. 2016, Journal of Molecular Spectroscopy, 327, 73

Tian, F. 2009, The Astrophysical Journal, 703, 905

Tigrine, S., Carrasco, N., Vettier, L., & Cernogora, G. 2016, Journal of Physics D: Applied Physics, 49, 395202

Tinetti, G., Drossart, P., Eccleston, P., et al. 2016, in Space Telescopes and Instrumentation 2016: Optical, Infrared, and Millimeter Wave, Vol. 9904, International Society for Optics and Photonics, 99041X

Tinetti, G., Drossart, P., Eccleston, P., et al. 2018, Experimental Astronomy, 46, 135

Trafton, L. M., Geballe, T., Miller, S., Tennyson, J., & Ballester, G. 1993, The Astrophysical Journal, 405, 761

Van Dishoeck, E. F., Herbst, E., & Neufeld, D. A. 2013, Chemical Reviews, 113, 9043

Venot, O., Agúndez, M., Selsis, F., Tessenyi, M., & Iro, N. 2014, Astronomy & Astrophysics, 562, A51

Verwer, J. G., & Sommeijer, B. P. 2004, SIAM Journal on Scientific Computing, 25, 1824

Vuitton, V., Flandinet, L., Orthous-Daunay, F.-R., et al. 2019a, in 2019 Astrobiology Science Conference, AGU

Vuitton, V., Yelle, R., Klippenstein, S., Hörst, S., & Lavvas, P. 2019b, Icarus, 324, 120

Wakelam, V., Herbst, E., Loison, J.-C., et al. 2012, The Astrophysical Journal Supplement Series, 199, 21

Waldmann, I. P., Rocchetto, M., Tinetti, G., et al. 2015a, The Astrophysical Journal, 813, 13

Waldmann, I. P., Tinetti, G., Rocchetto, M., et al. 2015b, The Astrophysical Journal, 802, 107

Wolters, C., Vuitton, V., Flandinet, L., et al. 2019, EPSC, 2019, EPSC

Wordsworth, R., & Pierrehumbert, R. 2014, The Astrophysical Journal Letters, 785, L20

Yelle, R. V. 2004, Icarus, 170, 167

Youngblood, A., France, K., Loyd, R. P., et al. 2016, The Astrophysical Journal, 824, 101

Yurchenko, S. N., Tennyson, J., Bailey, J., Hollis, M. D., & Tinetti, G. 2014, Proceedings of the National Academy of Sciences, 111, 9379